NJC

Accepted Manuscript

This is an *Accepted Manuscript*, which has been through the Royal Society of Chemistry peer review process and has been accepted for publication.

Accepted Manuscripts are published online shortly after acceptance, before technical editing, formatting and proof reading. Using this free service, authors can make their results available to the community, in citable form, before we publish the edited article. We will replace this *Accepted Manuscript* with the edited and formatted *Advance Article* as soon as it is available.

You can find more information about *Accepted Manuscripts* in the Information for Authors.

Please note that technical editing may introduce minor changes to the text and/or graphics, which may alter content. The journal's standard Terms & Conditions and the Ethical guidelines still apply. In no event shall the Royal Society of Chemistry be held responsible for any errors or omissions in this *Accepted Manuscript* or any consequences arising from the use of any information it contains.

ROYAL SOCIETY OF CHEMISTRY

www.rsc.org/njc

Lanthanide Metal − Organic Frameworks Based on 4,4′-oxybisbenzoic acid ligand: Synthesis, Structures and Physical Properties

Yun Li[a], Ning Wang[b], Yan-Ju Xiong[a], Qian Cheng[a], Jie-Fang Fang[a], Fei-Fei Zhu[a], Yi Long[b], Shan-Tang Yue[a*]

[a]*School of Chemistry and Environment, South China Normal University, Guangzhou 510006, PR China*

[b]*School of Materials Science and Engineering, Nanyang Technological University, Singapore 639798*

To whom correspondence should be addressed. E-mail: yuesht@scnu.edu.cn; Tel./fax: +86 20 39310187.

ABSTRACT: A series of lanthanide microporous coordination polymers, namely, $\{[Ln_4(OBA)_6(DMF)(H_2O)]\cdot 2DMF\cdot 3H_2O\}_n$ [Ln=Nd(**1**), Sm(**2**), Eu(**3**), Gd(**4**)]; $\{[Ln_4(OBA)_6(H_2O)_2]\cdot 3DMF\cdot 2H_2O\}_n$ [Ln=Tb(**5**), Dy(**6**)]; $\{[Ln_4(OBA)_6(DMF)(H_2O)_2]\cdot 2DMF\cdot 4H_2O\}_n$ [Ln=Tb(**7**), Dy(**8**)] (H_2OBA=4,4′-oxybisbenzoic acid, DMF= N,N′-dimethylformamide), have been successfully prepared via solvothermal methods and characterized by FT-IR, photoluminescent spectra, thermogravimetric analysis (TGA), powder X-ray diffraction (PXRD) and single-crystal X-ray diffraction. All of the lanthanide coordination polymers showed the three dimensional (3D) metal-organic frameworks. The structural variations in compounds **1**–**8** may be caused by lanthanide contraction and the different coordination modes of the V-shaped H_2OBA ligands. The luminescent properties of compounds **3**, **5** and **7** have been studied in the solid state at room temperature, and all of them displayed metal-based luminescence. Moreover, compounds **4**, **6** and **8** exhibited the antiferromagnetic coupling within the carboxyl oxygen bridged rare-earth chains.

Introduction

Metal–organic frameworks (MOFs)[1] including lanthanide ions have been paid tremendous attention during the past decades because of their potential applications in catalysis[2], magnetism[3], luminescent probes[4], gas storage[5] and separation[6] based on the diversity of structures and their physical/chemical properties. Previous studies[7] show that the choice of solvents and temperature plays a particularly important role in solvothermal synthesis, especially for particular structures and applications. The normal utilized solvents always refer to ethanol (EtOH), N,N′-dimethylformamide (DMF), N,N-dimethylacetamide (DMA), N,N-diethylformamide (DEF) and so on.

It is well known that flexible ligands could facilitate the self-assembly of high dimensional and complicated MOFs[8]. Several lanthanide-containing MOFs have already been synthesized in solvothermal methods by using water or e-urea as solvents and 4,4′-oxybisbenzoic acid as the ligand[4b,8a,9]. To the best of our knowledge, the selection of DMF solvent only as well as H_2OBA ligand to synthesis lanthanide 3D Metal–organic frameworks has not been reported yet[9].

As a V-shaped ligand, H_2OBA contains two carboxylate groups, which could help to obtain coordination frameworks with higher dimensions and interesting topologies [9d,10]. With this in mind, we try to select DMF as the solvent and H_2OBA as the ligand to obtain porous MOFs. In this paper, we report the assembly of a series of lanthanide microporous MOFs through the solvothermal reaction between the lanthanide salts and H_2OBA ligands in DMF solvent, and present their luminescent and magnetic properties.

Experimental section

Materials and general methods. The ligand H_2OBA was buying from Jinan Henghua Sci. & Tec. Co. Ltd. and other materials were commercially available used without further purification. Elemental analyses for C, H, N were performed on a Elementar Vario EL CUBE analytical instrument. The FT-IR spectra were recorded from KBr pellets in the 4000-500 cm^{-1} ranges on a Nicolet 5DX spectrometer. Thermogravimetric analyses were performed on Perkin-Elmer TGA 7 analyzer with a heating rate of 10˚C min^{-1} in flowing N_2 atmosphere. The luminescent spectra for the solid state were recorded at room temperature on Hitachi F-2500 and Edinburgh-FLS-920 with a xenon arc lamp as the light source. Powder X-ray diffraction (PXRD) patterns were recorded on a X-pert diffractometer or Rigaku D/M-2200T automated diffractometer for Cu Kα radiation (λ = 1.54060 Å), with a scan speed of 4˚ min^{-1} and a step size of 0.02˚ in 2θ range of 5-40˚. The magnetic susceptibility measurements were carried out on polycrystalline samples on a Quantum Design MPMS-XL5 SQUID magnetometer in the temperature range of 2-300 K. Diamagnetic corrections were estimated from Pascal's constants for all constituent atoms.

Synthesis of $\{[Nd_4(OBA)_6(DMF)(H_2O)]\cdot 2DMF\cdot 3H_2O\}_n$(1)

A mixture of $Nd(NO_3)_3\cdot 6H_2O$ (0.1mmol), 4,4′-oxybisbenzoic acid (H_2OBA) (0.3mmol), and DMF (2mL) was placed in a 23 mL Teflon-lined stainless steel vessel. The mixture was sealed and heated at 160˚C for three days, and then cooled to room temperature at a rate of 5˚C/h. Purple columnar-shaped crystals suitable for X-ray analysis were obtained with 61% (based on the H_2OBA). Found/calcd: C, 46.47/46.43%; H 3.56/3.23% ; N 1.80/1.75%. IR (KBr, cm^{-1}): 3071(w), 2930(w), 1659(s), 1593(s), 1531(s), 1500(w), 1393(s), 1304(w), 1238(s), 1160(m), 1097(w), 1012(w), 880(m), 802(s), 784(m), 767(w), 697(m), 657(w).

Synthesis of $\{[Sm_4(OBA)_6(DMF)(H_2O)]\cdot 2DMF\cdot 3H_2O\}_n$(2)

The process was same as **1** except that the $Nd(NO_3)_3\cdot 6H_2O$ was replaced by $Sm(NO_3)_3\cdot 6H_2O$ (0.1mmol). Pale yellow columnar-shaped crystals suitable for X-ray analysis were obtained with 64% (based on the H_2OBA). Found/calcd: C, 45.58/45.96%; H 3.31/3.19% ; N 1.84/1.73%. IR (KBr, cm^{-1}): 3069(w), 2928(w), 1659(s), 1594(s), 1530(s), 1501(w), 1397(s), 1305(w), 1241(s), 1161(m), 1099(w), 1012(w), 880(m), 803(s), 784(m), 767(w), 697(m),

658(w).

Synthesis of $\{[Eu_4(OBA)_6(DMF)(H_2O)]\cdot 2DMF\cdot 3H_2O\}_n$(3)

The process was same as **1** except that the $Nd(NO_3)_3\cdot 6H_2O$ was replaced by $Eu(NO_3)_3\cdot 6H_2O$ (0.1mmol). White columnar-shaped crystals suitable for X-ray analysis were obtained with 68% (based on the H_2OBA). Found/calcd: C, 44.90/45.84%; H 3.17/3.19% ; N 1.47/1.72%. IR (KBr, cm^{-1}): 3074(w), 2928(w), 1660(s), 1594(s), 1532(s), 1505(w), 1397(s), 1305(w), 1241(s), 1161(m), 1099(w), 1012(w), 881(m), 803(s), 784(m), 767(w), 698(m), 657(w).

Synthesis of $\{[Gd_4(OBA)_6(DMF)(H_2O)]\cdot 2DMF\cdot 3H_2O\}_n$(4)

The process was same as **1** except that the $Nd(NO_3)_3\cdot 6H_2O$ was replaced by $Gd(NO_3)_3\cdot 6H_2O$ (0.1mmol). White columnar-shaped crystals suitable for X-ray analysis were obtained with 67% (based on the H_2OBA). Found/calcd: C, 44.82/45.45%; H 3.19/3.16% ; N 1.57/1.71%. IR (KBr, cm^{-1}): 3074(w), 2930(w), 1660(s), 1594(s), 1532(s), 1505(w), 1394(s), 1304(w), 1240(s), 1161(m), 1098(w), 1012(w), 881(m), 803(s), 784(m), 767(w), 698(m), 657(w).

Synthesis of $\{[Tb_4(OBA)_6(H_2O)_2]\cdot 3DMF\cdot 2H_2O\}_n$(5)

The process was same as **1** except that the $Nd(NO_3)_3\cdot 6H_2O$ was replaced by $Tb(NO_3)_3\cdot 6H_2O$ (0.1mmol). White columnar-shaped crystals suitable for X-ray analysis were obtained with 69% (based on the H_2OBA). Found/calcd: C, 44.91/45.32%; H 3.19/3.15% ; N 1.77/1.71%. IR (KBr, cm^{-1}): 3071(w), 2930(w), 1662(s), 1594(s), 1532(s), 1502(w), 1397(s), 1304(w), 1239(s), 1161(m), 1097(w), 1012(w), 880(m), 802(s), 784(m), 767(w), 697(m), 657(w).

Synthesis of $\{[Dy_4(OBA)_6(H_2O)_2]\cdot 3DMF\cdot 2H_2O\}_n$(6)

The process was same as **1** except that the $Nd(NO_3)_3\cdot 6H_2O$ was replaced by $Dy(NO_3)_3\cdot 6H_2O$ (0.1mmol). White columnar-shaped crystals suitable for X-ray analysis were obtained with 54% (based on the H_2OBA). Found/calcd: C, 44.24/45.06%; H 3.32/3.13% ; N 1.82/1.70%. IR (KBr, cm^{-1}): 3069(w), 2930(w), 1661(s), 1594(s), 1532(s), 1505(w), 1393(s), 1304(w), 1240(s), 1162(m), 1099(w), 1012(w), 880(m), 802(s), 784(m), 766(w), 697(m), 657(w).

Synthesis of $\{[Tb_4(OBA)_6(DMF)(H_2O)_2]\cdot 2DMF\cdot 4H_2O\}_n$(7)

The process was same as **5**. White block-shaped crystals suitable for X-ray analysis were obtained with 51% (based on the H_2OBA). Found/calcd: C, 44.54/44.67%; H 3.15/3.27% ; N 1.46/1.68%. IR (KBr, cm^{-1}): 3072(w), 2928(w), 1660(s), 1595(s), 1535(s), 1505(w), 1393(s),

1305(w), 1248(s), 1163(m), 1101(w), 1012(w), 881(m), 800(s), 783(m), 767(w), 697(m), 664(w).

Synthesis of $\{[Dy_4(OBA)_6(DMF)(H_2O)_2]\cdot 2DMF\cdot 4H_2O\}_n$(8)

The process was same as **6**. White block-shaped crystals suitable for X-ray analysis were obtained with 58% (based on the H_2OBA). Found/calcd: C, 44.74/44.42%; H 3.20/3.25% ; N 1.83/1.67%. IR (KBr, cm^{-1}): 3072(w), 2925(w), 1660(s), 1595(s), 1538(s), 1505(w), 1341(s), 1305(w), 1247(s), 1163(m), 1100(w), 1012(w), 882(m), 800(s), 783(m), 769(w), 697(m), 665(w).

X-Ray crystallography

Single crystal X-ray diffraction data collections of **1**–**8** were performed on a Bruker APEX II CCD diffractometer operating at 50 kV and 30 mA using Mo Kα radiation (λ = 0.71073 Å) at 293-298 K. Data collection and reduction were performed using the APEX II software. Multi-scan absorption corrections were applied for all the data sets using the APEX II program. All eight structures were solved by direct methods and refined by full-matrix least squares on F^2 using the SHELXTL program package. All nonhydrogen atoms were refined with anisotropic displacement parameters. Hydrogen atoms attached to carbon were placed in geometrically idealized positions and refined using a riding model. Hydrogen atoms on water molecules were located from difference Fourier maps and were also refined using a riding model. It should be mentioned that the highly disordered guest molecules was speculated by analysis the TGA results, the residual electron density calculated by PLATON/SQUEEZE[11] combine with element analysis and included in the molecular formula directly. The crystallographic data and refinement parameters of **1**–**6** are listed in Table S1, **7**–**8** are listed in Table S2 and selected bond lengths (Å) for complexes **1**, **2**, **5**, **6**, **7** and **8** in Table S3.

.

Results and discussion

Crystal structures of compounds 1–6

Single-crystal X-ray analyses reveal that **1**–**6** crystallize in the triclinic space group *P*-1 and present 3D coordination frameworks. The structures of **1**–**6** are remarkably similar with almost the same crystallographic data and refinement parameters except that the four crystallographically independent Tb (III) atoms in **5** and Dy (III) atoms in **6** are all eight-coordinated with no DMF participated in the coordination. So only the structure of **1** is described in detail. Each independent asymmetric unit contains four Nd (III) atoms, six OBA^{2-} molecules, one DMF and one coordinated water. As depicted in Fig. 1a, the four crystallographically independent Nd (III) atoms have different coordination geometries. Nd1 and Nd2 atoms are eight-coordinated, while Nd3 and Nd4 are nine-coordinated. Nd1 form a dodecahedron geometric configuration and coordinated by four oxygen atoms from two chelate carboxylate group of an OBA^{2-} ligand, and four oxygen atoms from bidentate carboxylate groups of OBA^{2-} ligands. The Nd1–O bond lengths vary from 2.372(8) to 2.842(7)

Å and the O–Nd1–O bond angles range from 76.46(0)˚ to 159.28(2)˚. Similarly, Nd2 is eight-coordinated and has a dodecahedron geometric configuration constituted of two oxygen atoms from one chelate carboxylate group of an OBA^{2-} ligand, five oxygen atoms from bidentate carboxylate groups of OBA^{2-} ligands and one oxygen atom from coordinated DMF. The Nd2–O bond lengths vary from 2.388(7) to 2.764(8) Å and the O–Nd2–O bond angles range from 66.97(1)˚ to 147.82(6)˚. Nd3 is coordinated by three oxygen atoms from three bidentate carboxylate groups of OBA^{2-} ligands, and six oxygen atoms from three chelate carboxylate group of an OBA^{2-} ligand, forming a tetrakaidecahedron geometric configuration. The Nd3–O bond lengths vary from 2.367(8) to 2.598(6) Å and the O–Nd3–O bond angles are in the range of 81.45(3)˚ and 166.77(4)˚. Analogously, Nd4 is coordinated by four oxygen atoms from four bidentate carboxylate groups of OBA^{2-} ligands, four oxygen atoms from two chelate carboxylate group of an OBA^{2-} ligand and one coordinated oxygen atom to furnish a tetrakaidecahedron geometric configuration. The Nd4–O bond lengths vary from 2.286(8) to 2.716(7) Å and the O–Nd4–O bond angles lie in the range of 48.4(2)˚ and 171.5(3)˚. Each independent asymmetric unit connects both ends (Nd1···Nd2···Nd3···Nd4···Nd1···Nd2···Nd3···Nd4) to result in a chain (Fig. 1b and indicate by polyhedral in Fig.S1). These chains are further interlinked by the organic bridges to produce two-dimensional layer structures (Fig. 1c and Fig. S1). It should be noted that the two two-dimensional (2D) layer in Fig. 1c dislocation connected each other to complete the construction of the three-dimensional (3D) framework (Fig. 1d). After the guest molecules are removed from the channels, PLATON calculations show that the accessible volume is 1495.0 $Å^3$ (29.0%) per unit cell volume.

.

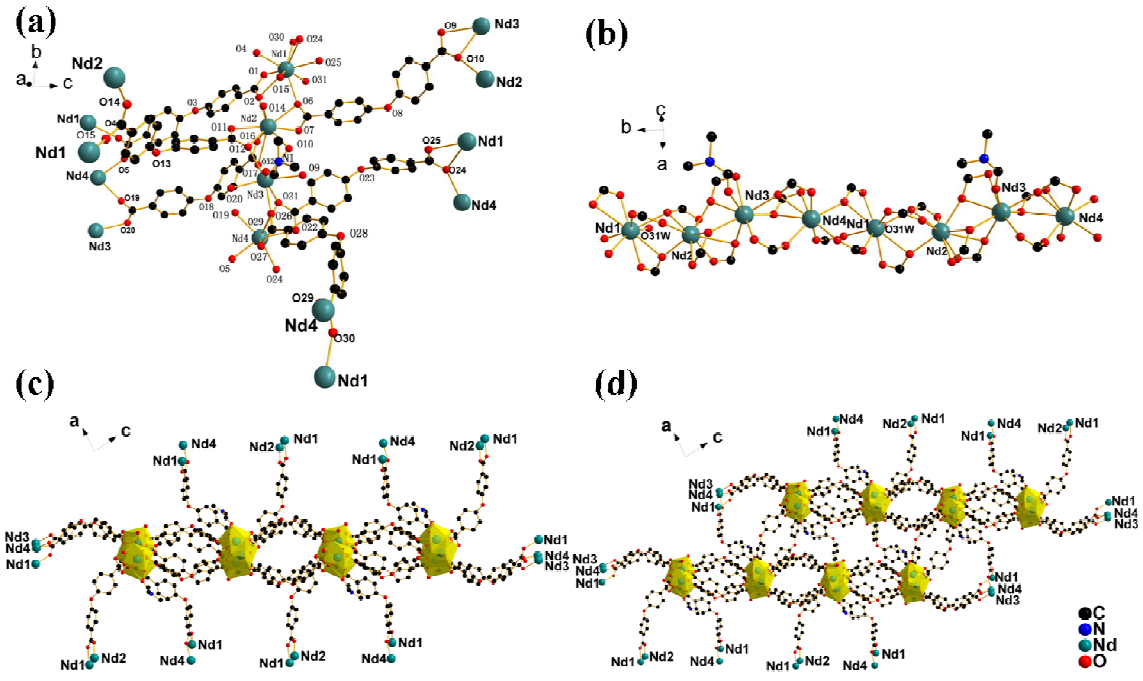

Fig. 1 (a) The coordination environment in **1**. (b) The metal-chain in **1**. (c) The two-dimensional porous network layer in **1**. (d) View of the three-dimensional architecture of **1**. (Hydrogen omitted for clarity)

Crystal structures of compounds 7–8

The single crystal X-ray diffraction studies revealed that compounds **7** and **8** are isostructural

with space group of $P2_1/n$ and 3D coordination frameworks, which are different from the two types of frameworks mentioned above (**1**–**6**). Although using the identical synthesized method, compound **7** and **8** are of block-shaped crystals while compounds **5** and **6** are columnar-shaped. Herein only the structure of **7** is described in detail. Each independent asymmetric unit contains four Tb (III) atoms, six OBA^{2-} molecules and two aqua ligands and one DMF ligand. As depicted in Fig. 2a, compared to frameworks **1**–**6**, the four crystallographically independent Tb (III) atoms have three different coordination numbers. Tb1 and Tb3 are eight-coordinated, Tb2 is nine-coordinated and Tb4 is seven-coordinated. Tb1 is coordinated by six oxygen atoms from bidentate carboxylate groups of OBA^{2-} ligands, one oxygen atom from one DMF ligand and one oxygen atom from one aqua ligand. The Tb1–O bond lengths vary from 2.233(7) to 2.612(0) Å and the O–Tb1–O bond angles range from 47.8(2)˚ to 167.7(3)˚. Tb2 is coordinated by three oxygen atoms from the bidentate carboxylate groups of OBA^{2-} ligands, six oxygen atoms from three chelate carboxylate group of an OBA^{2-} ligand. The Tb2–O bond lengths vary from 2.301(6) to 2.612(6) Å and the O–Tb2–O bond angles range from 52.39(4)˚ to 153.02(9)˚. The eight-coordinated Tb3 forming a dodecahedron geometric configuration is coordinated by four oxygen atoms from two chelate carboxylate group of OBA^{2-} ligand, four oxygen atoms from bidentate carboxylate groups of OBA^{2-} ligands. The Tb3–O bond lengths vary from 2.221(7) to 2.603(6) Å and the O–Tb3–O bond angles range from 75.79(1)˚ to 147.71(0)˚. Tb4 is coordinated by six oxygen atoms from bidentate carboxylate groups of OBA^{2-} ligands and one oxygen atom from aqua molecule. The Tb4–O bond lengths vary from 2.267(8) to 2.414(1) Å and the O–Tb4–O bond angles range from 68.81(1)˚ to 167.66(6)˚. Each independent asymmetric unit connects both ends (Tb1···Tb2···Tb3···Tb4···Tb1···Tb2···Tb3···Tb4) to result in a chain (Fig. 2b and indicate by polyhedral in Fig.S2). These chains are further interlinked by the organic bridges to produce two-dimensional layer structures (Fig. 2c and Fig. S2). It can be seen that the two-dimensional layer in Fig. 2c rotary itself 180˚, and then connected to its own displacement, then we got the three-dimensional (3D) framework (Fig. 2d). After the guest molecules were removed from the channels, PLATON calculations show that the accessible volume is 2618.1 $Å^3$ (26.0%) per unit cell volume.

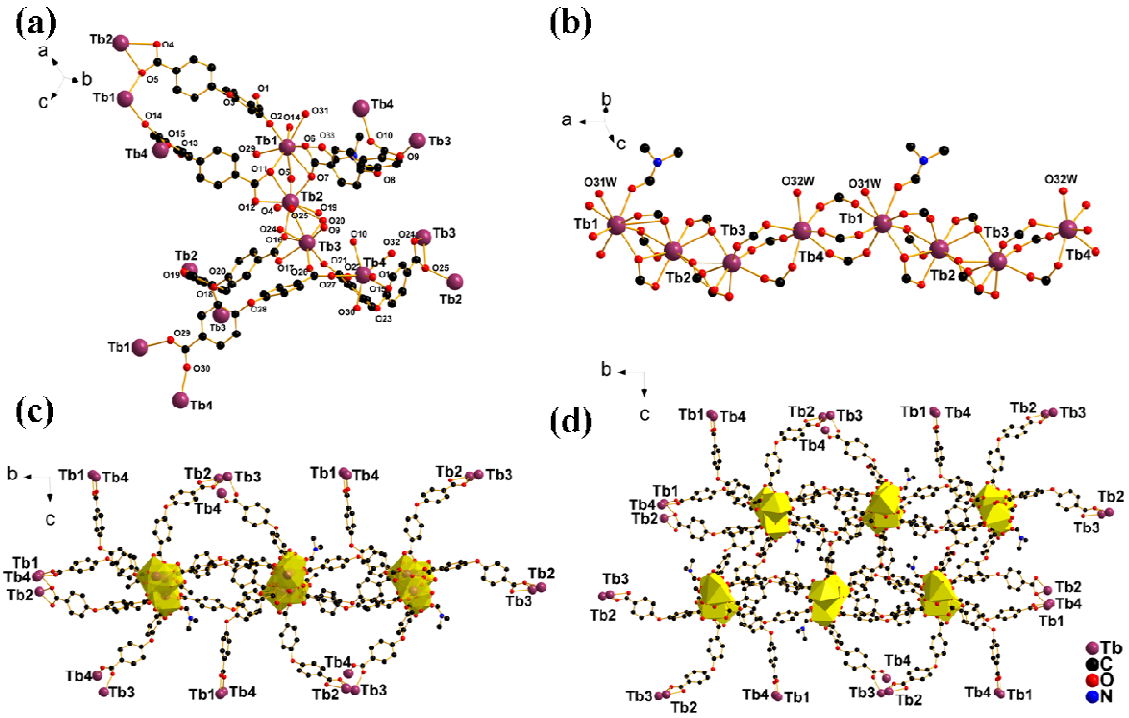

Fig. 2 (a) The coordination environment in **7**. (b) The metal-chain in **7**. (c) The two-dimensional porous network layer in **7**. (d) View of the three-dimensional architecture of **7**. (Hydrogen omitted for clarity)

Structural diversity of the compounds

The effects of lanthanide contraction always exist in lanthanide-ions-based MOFs[12]. The effect can result in a regularly structural diversity and it also plays a significant part in the structure of compounds **1**–**8** we have prepared. From the structure analyzed above, it can concluded the main impact of lanthanide contraction is the coordination number of Ln ion and the average bond length of Ln–O decreases with the radius of Ln ions decreasing[13] and the detail are summarized in Table 1. What's more, we found that DMF molecules participated in coordinating with compounds **1**–**4**, while no DMF molecules coordinated with complexes **5** and **6** which is not only because DMF molecule is larger than H_2O molecule but also due to the fact that the radius of Ln (III) ions in compound **5** and **6** are shorter than Ln (III) ions in **1**–**4** compounds. Moreover, only Tb (III) and Dy (III) with two different structures were obtained at the same process, these may be attributed to the influence of lanthanide contraction.

Besides, the structural diversity of compounds **1**–**8** were also affected by the V-shaped flexible H_2OBA ligand. Various coordination modes of OBA^{2-} ligands are showed in the structures of **1**–**8**. In **1**–**4**, two OBA^{2-} ligands adopt chelate-bridging coordination modes (Fig. 3a), four OBA^{2-} ligands adopt chelate-bridging and μ^2-bridging combination coordination modes (Fig. 3b). In **5** and **6**, one OBA^{2-} ligand adopts chelate-bridging coordination modes (Fig. 3a), four OBA^{2-} ligands adopt chelate-bridging and μ^2-bridging combination coordination modes (Fig. 3b), and one OBA^{2-} ligand adopts μ^2-bridging coordination modes (Fig. 3c). In **7** and **8,** one OBA^{2-} ligand adopts chelate-bridging coordination modes (Fig. 3a),

three OBA^{2-} ligands adopt chelate-bridging and μ^2-bridging combination coordination modes (Fig. 3b), and two OBA^{2-} ligands adopt μ^2-bridging coordination modes (Fig. 3c).

Table 1. The coordination number and the average bond length (Ln–O) of **1**–**8**. (8 + 8 + 9 + 9 is a representation of the coordination numbers of the four metal centers in each compound).

complex	1	2	3	4	5	6	7	8
Coordination numbers	8 + 8 + 9 + 9				8 + 8 + 8 + 8		7 + 8 + 9 + 8	
average bond length Å（Ln–O）	2.492(6)	2.463(4)	2.451(2)	2.449(1)	2.415(0)	2.394(3)	2.388(7)	2.383(1)

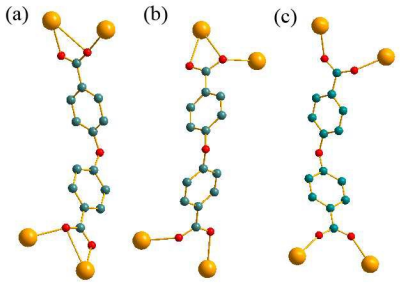

Fig. 3 The different coordination modes of H_2OBA ligands.

PXRD, IR and Thermal stability analysis

The as-isolated samples of the complexes were characterized by powder X-ray diffraction at room temperature (Fig. 4). When compared to the simulated patterns based on the single crystal data samples, the experimental patterns are well in agreement with the calculated diffractograms, thus basically pointing toward the formation of only a single phase product under the reaction conditions employed for these complexes. IR spectrum of complex **1**–**8** showed in Fig. S6–S13.

The thermal stabilities of **1**–**8** were investigated on polycrystalline samples by the thermogravimetric analyses (TGA) under N_2 atmosphere with a heating rate of 10˚C min^{-1} from RT to 750˚C. On account of the remarkably similar features of **1**–**6**, **1** is described in detail as a typical example. The TG trace for **1** reveals that the guest molecules in the channel and the coordinated solvents molecules are gradually removed and weight loss of 10.5% in proceeding from 35˚C to 260˚C. Above 450˚C, the weight loss is due to the decomposition of the organic ligands. As shown in Fig. S3 and S4. The TG curves of **7** and **8** are similar to **1**–**6** (see Fig. S5), guest molecules in the channel and the coordinated solvents molecules are gradually removed in proceeding from 35˚C to 260˚C and the observed weight loss was 10.4%. Above 450˚C, the whole framework begins to collapse due to the decomposition of the organic ligands.

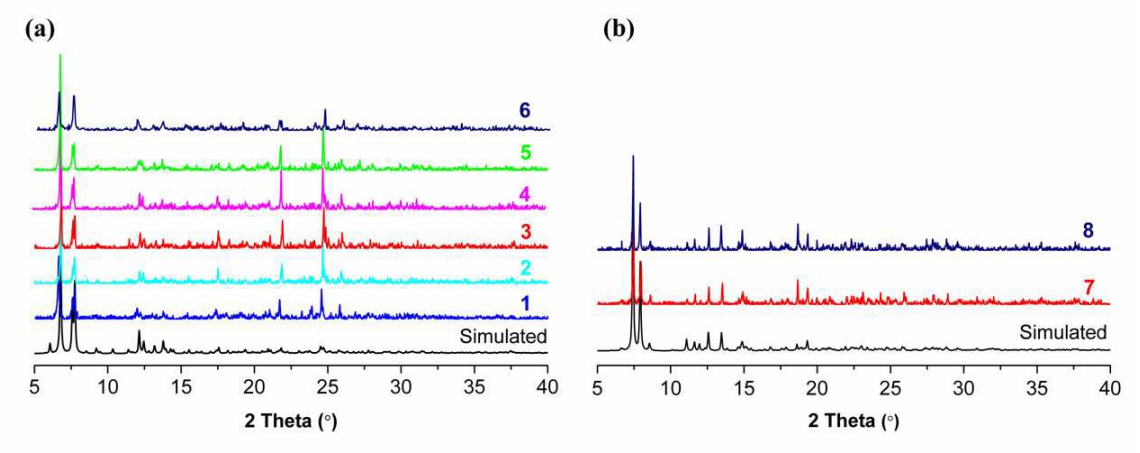

Fig. 4 (a) PXRD of Complex **1**–**6**. (b) PXRD of Complex **7** and **8**.

Luminescent properties

Due to the excellent photoluminescence properties of the lanthanide compounds, the luminescence of **3**, **5** and **7** containing Eu (III) and Tb (III) ions was investigated in the solid state. As shown in Fig. 5a, the emission spectrums of **3** upon excitation at 395 nm exhibit the characteristic transition of Eu (III) ion. They are attributed to $^5D_0 \rightarrow {}^7F_J$ (J=0→4) transitions, i.e. 579 nm ($^5D_0 \rightarrow {}^7F_0$), 592 nm ($^5D_0 \rightarrow {}^7F_1$), 613 and 619 nm ($^5D_0 \rightarrow {}^7F_2$), 654 nm ($^5D_0 \rightarrow {}^7F_3$), and 704 nm ($^5D_0 \rightarrow {}^7F_4$). The $^5D_0 \rightarrow {}^7F_2$ transition is stronger than that of $^5D_0 \rightarrow {}^7F_1$ transition, indicating that Eu (III) ions have a low symmetric coordination environment without an inversion center. These transitions are consistent with the result of the single-crystal X-ray analyses. Compound **5** and **7** yield green light and exhibit the characteristic emission of $^5D_4 \rightarrow {}^7F_J$ (J = 3→6) of the Tb (III) ion (Fig. 5b). Two intense emission bands at 489 and 544 nm are attributed to $^5D_4 \rightarrow {}^7F_6$ and $^5D_4 \rightarrow {}^7F_5$, respectively, while the weaker emission bands at 590 nm and 619 nm originate from $^5D_4 \rightarrow {}^7F_4$ and $^5D_4 \rightarrow {}^7F_3$. Difference of luminescent intensity in compound **5** and **7** can be ascribed to different coordinated solvent molecules in **5** and **7**. Evidently, there are one DMF and two water molecules coordinated to Tb (III) ions in each independent asymmetric unit in compound **7** while there is only two water molecules coordinated to Tb (III) ions in compound **5** at each independent asymmetric unit. It is well known that the small coordinated molecules H_2O and DMF enter the coordination spheres of the terbium ions within the framework that quenches the luminescence intensities effectively[14]. In this sense the effect of coordinated molecules on compound **7** is much more obvious than that of compound **5**. Therefore, the Tb-centered luminescence of compound **5** outperformed that of **7**.

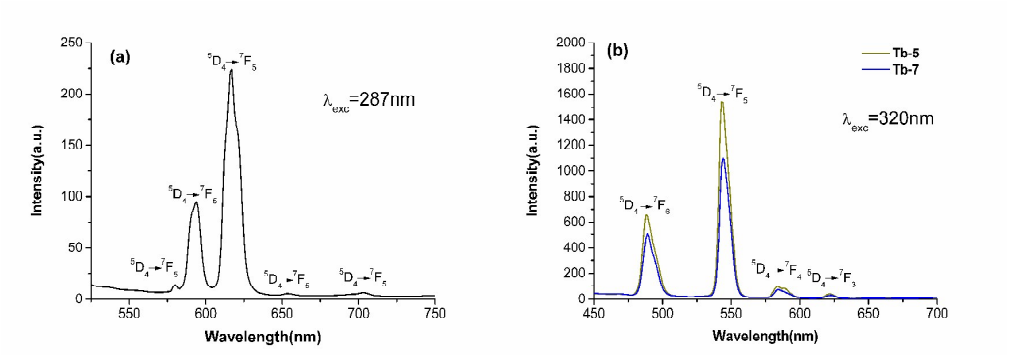

Fig. 5 (a) Luminescent spectra of compounds **3**. (b) Luminescent spectra of compounds **5** and **7**.

Magnetic property

The solid state magnetic susceptibility measurement for compounds **4**, **6** and **8** has been performed in the temperature range 2 to 300 K under the field of 1000 Oe, and the data have been recorded as plots of $\chi_M T$ versus T as well as $1/\chi_M$ versus T where χ_M is the molar magnetic susceptibility. As shown in Fig 6, the room temperature $\chi_M T$ value for **4**, **6** and **8** is 29.08 cm^3Kmol^{-1}, 51.12 cm^3Kmol^{-1} and 52.66 cm^3Kmol^{-1}, slightly lower than that of their respective spin-only Gd_4 ($^8S_{7/2}$, g_J=2, J=7/2), Dy_4 ($^6H_{15/2}$, g_J=4/3, J=15/2) units in one molar molecule. Due to the large distance (> 13 Å) between the RE cations in **4**, **6** and **8**, separated by the H_2OBA ligands, the magnetic structures can be simplified as carboxyl-oxygen connected 1D chains with average RE-RE distance 3.92 Å, 3.97 Å and 4.08 Å, respectively. The $\chi_M T$ data were reproduced using the uniform chain mode[15],

$$\chi_M = Ng^2\beta^2/3kT \cdot (1+u)/(1-u),$$

$$u = \coth[JS(S+1)/kT] - kT/JS(S+1) \quad (1),$$

Where J/cm^{-1} is the coupling strength between the neighboring paramagnetic cations within the chain. The best fitting result above 50K for **4**, **6** and **8** is g_J=1.9, J= –0.01 cm^{-1}; g_J=1.26, J= –0.08 cm^{-1} and g_J=1.28, J=–0.07 cm^{-1}; respectively. The little negative J value revealed the weak antiferromagnetic coupling between the RE cations through carboxyl-oxygen connections within 1D chains, which can also be qualitatively deduced from the gradually depression of $\chi_M T$ in the cooling process. In addition, the $1/\chi_M$ data above 50 K can be simulated by the Curie-Weiss law $\chi_M = C/(T-\theta)$ with Weiss constant θ=–1.83 K, –6.94 K and –5.66 K for **4**, **6** and **8**, respectively, also indicating the weak antiferromagnetic couplings within the 1D chain.

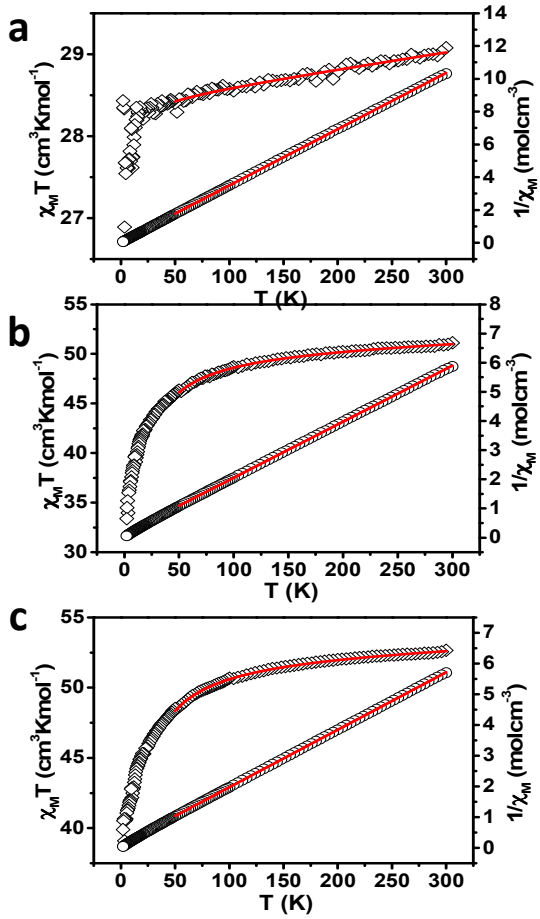

Fig. 6 Plots of $\chi_M T$ versus T and $1/\chi_M$ versus T for compounds **4** (a), **6** (b) and **8** (c). The solid lines represent the best fitting results as described in the text.

Conclusion

To conclude, a series of lanthanide MOFs with three-dimensional microporous structures based on the H_2OBA ligands and Ln (III) ion have been successfully synthesized. The result revealed that the lanthanide contraction and the solvents of DMF play vital roles in the flexible construction of lanthanide MOFs. A reasonable explanation has been proposed to demonstrate the structure flexibility of compounds **5**–**8**. Since this phenomenon only occurs at MOFs based on Tb (III) and Dy (III) ion, it should be rational to assume that solvothermal reaction is hard to control under high temperature & high pressure and the lanthanide contraction should play a critical role in the construction of lanthanide MOFs. Moreover, compounds **3**, **5** and **7** exhibited attractive luminescent properties and compounds **4**, **6** and **8** showed weak antiferromagnetic couplings within the lanthanide chains through the carboxyl oxygen bridging.

Acknowledgments

This work was financially supported by the National Nature Science Foundation of China (20971047, 21271076 and 21471060), Key Program of Guangdong Universities Science and Technology innovation (cxzd1020), and Planning Program of Guangzhou City Science and Technology (2013J4100049).

References

[1] (a) Special Issue on MOFs. *Chem. Soc. Rev.*, **2009**, 38, 1201;
(b) Special Issue on MOFs. *Chem. Rev.*, **2012**, 112, 673.

[2] (a) F. G andara, A. Garc ıa-Cort es, C. Cascales, B. Gomez-Lor, E. Guti errez-Puebla, M. Iglesias, A. Monge and N. Snejko, *Inorg. Chem*., **2007**, 46, 3475;
(b) F. G andara, C. Fortes-Revilla, N. Snejko, E. Guti errez-Puebla, M. Iglesias and A. Monge, *Inorg. Chem.*, **2006**, 45, 9680.

[3] (a) Okazawa. A, Nogami. T, Nojiri. H, Ishida. T, *Chem. Mater.,* **2008**, 20, 3110;
(b) Aronica. C, Chastanet. G, Pilet. G, Guennic. B, Robert. L. V, Wernsdorfer. W, Luneau. D, *Inorg. Chem.,* **2007**, *46*, 6108;
(c) Chandrasekhar.V, Pandian. B. M, Boomishankar. R, Steiner. A, Vittal. J. J, Houri. A, Clerac. R, *Inorg. Chem.,* **2008**, 47, 4919;
(d) Zhang. J. J, Hu. S. M., Xiang. S. C, Sheng. T. L, Wu. X. T, Li. Y. M, *Inorg. Chem.,* **2006**, 45, 7173.

[4] (a) B. Zhao, X.-Y. Chen, P. Cheng, D.-Z. Liao, S.-P. Yan, Z.-H. Jiang, *J. Am. Chem. Soc.,* **2004**, 126, 15394;
(b) Y.-W. Lin, B.-R. Jian, Sin-C hiang Huang, Chin-Her Huang, Kuei-Fang Hsu, *Inorg. Chem.*, **2010**, 49, 2316.

[5] (a) Morris. R. E, Wheatley. P. S, *Angew. Chem.,* **2008**, 120, 5044;
(b) Suh. M. P, Park. H. J, Prasad. T. K, Lim. D.-W, *Chem. Rev*., **2012**, 112, 782;
(c) Ma. S. Pure, *Appl. Chem.,* **2009**, 81, 2235.

[6] (a) Pan. L, Parker. B, Huang. X, Olson. D. H, Lee. J. Y, Li. J, *J. Am. Chem. Soc.,* **2006**, 128, 4180;
(b) Pan. L, Adams. K. M, Hernandez. H. E, Wang. X, Zheng. C, Hattori. Y, Kaneko. K, *J. Am. Chem. Soc.,* **2003**, 125, 3062;
(c) Matsuda. R, Kitaura. R, Kitagawa. S, Kubota. Y, Belosludov. R. V, Kobayashi. T. C, Sakamoto. H, Chiba. T, Takata. M, Kawazoe. Y, Mita. Y, *Nature,* **2005**, 436, 238;
(d) Dinca. M, Long. J. R, *J. Am. Chem. Soc.,* **2005**, 127, 9376.

[7] (a) R. E. Morris, *Chem. Commun.*, **2009**, 25, 2990;
(b) R. E. Morris and S. J. Weigel, *Chem. Soc. Rev.*, **1997**, 26, 309;
(c) M.-W. Zhang, Y.-P. Chen, M. Bosch, T. Gentle III, K.-C. Wang, D.-W. Feng, Z.-Y. Wang and H.-C. Zhou, *Angew. Chem. Int. Ed.*, **2014**, 53, 815;

(d) Y.-B. Zhang, W.-X. Zhang, F.-Y. Feng, J.-P. Zhang, X.-M. Chen, *Angew. Chem. Int. Ed.*, **2009**, 48, 5287.

[8] (a) Y. Luo, Y.-J. Zheng, G. Calvez, S. Freslon, K. Bernot, C. Daiguebonne, T. Roisnel, O. Guillou, *CrystEngComm,* **2013**, 15, 706;
(b) O. Guillou and C. Daiguebonne, in *Handbook on the Physics and Chemistry of Rare Earths*, ed. K. A. Gschneider, J. C. G. Bu ¨nzli and V. K. Pecharsky, Elsevier, Amsterdam, **2005**, 34, 359.

[9] (a) P. C. Rao, Asha K. S, S. Mandal, *CrystEngComm*, **2014**, 16, 9320;
(b) Z.-Q. Jiang, G.-Y. Jiang, D.-C. Hou, F. Wang, Z. Zhao, J. Zhang, *CrystEngComm*, **2013**, 15, 315;
(c) Y. Qiu, C. Daiguebonne, J. Liu, R. Zeng, N. Kerbellec, H. Deng, O. Guillou, *Inorg. Chim. Acta.*, 2007, 360, 3265;
(d) R. Łyszczek, L. Mazur, *Inorg. Chem. Commun.*, **2012**, 15, 121;
(e) Y.-F. He, D.-M. Chen, H. Xu, P. Cheng, *CrystEngComm*, **2015**, 17, 2471.

[10] (a) P. Mahata, A. Sundaresan and S. Natarajan, *Chem. Commun.*, **2007**, 4471;
(b) M. Kondo, Y. Irie, Y. Shimizu, M. Miyazawa, H. Kawaguchi, A. Nakamura, T. Naito, K. Maeda, F. Uchida, *Inorg. Chem.*, **2004**, 43, 6139;
(c) F. Wang, X. Ke, J. Zhao, K. Deng, X. Leng, Z. Tian, L. Wen and D. Li, *Dalton Trans.*, **2011**, 40, 11856;
(d) Z.-B. Han, X.-N. Cheng and X.-M. Chen, *Cryst. Growth Des.*, **2005**, 5, 695.

[11] Spek, A.L. *J. Appl. Crystallogr.*, **2003**, 36, 7.

[12] (a) Y.-F. Zhou, F.-L. Jiang, D.-Q. Yuan, et al. *Angew. Chem. Int. Ed.*, **2004**, 43, 5665;
(b) B. Zhao, P. Cheng, X.-Y. Chen, et al. *J. Am. Chem. Soc.*, **2004**, 126, 3012;
(c) L. Pan, K. M. Adams, H. E. Hernandez, et al. *J. Am. Chem. Sco.*, **2003**, 125, 3062.

[13] (a) W.-T Xu, Y.-F. Zhou, M.-C. Hong, *Cryst. Growth Des*., **2013**, 13, 5420;
(b) J.-X. Liu, Y.-F. Hu, X.F. Chu, *CrystEngComm*, **2012**, 14, 6983.

[14] (a) F. S. Richardson, *Chem. Rev.*, **1982**, 82, 541;
(b) J.-C. G, Bünzli, Piguet, *C. Chem. Rev.*, **2002**, 102, 1897.

[15] M.E. Fisher, *Am. J. Phys*., **1964**, 32, 343.

Supporting Information Available: Crystallographic data for **1-8** in CIF format, TG&IR curves for **1-8**, selected bond lengths (Å) date.

Using solvothermal synthesis, eight new 3D microporous lanthanide-ions-based MOFs constructed from 4,4′-oxybisbenzoic acid were obtained and displayed two type of architecture.